







Biallelic CACNA2D1 loss-of-function variants cause early-onset developmental epileptic encephalopathy

Shehrazade Dahimene,¹ Leonie von Elsner,² Tess Holling,² Lauren S. Mattas,³ Jess Pickard,¹  Davor Lessel,² Kjara S. Pilch,¹ Ivan Kadurin,¹ Wendy S. Pratt,¹  Igor B. Zhulin,⁴ Hongzheng Dai,⁵ Maja Hempel,² Maura R. Z. Ruzhnikov,³  Kerstin Kutsche^{2,†} and  Annette C. Dolphin^{1,†}

[†]These authors contributed equally to this work.

Voltage-gated calcium (Ca_v) channels form three subfamilies (Ca_v1–3). The Ca_v1 and Ca_v2 channels are heteromeric, consisting of an α₁ pore-forming subunit, associated with auxiliary Ca_vβ and α₂δ subunits. The α₂δ subunits are encoded in mammals by four genes, CACNA2D1–4. They play important roles in trafficking and function of the Ca_v channel complexes. Here we report biallelic variants in CACNA2D1, encoding the α₂δ-1 protein, in two unrelated individuals showing a developmental and epileptic encephalopathy. Patient 1 has a homozygous frameshift variant c.818_821dup/p.(Ser275Asnfs*13) resulting in nonsense-mediated mRNA decay of the CACNA2D1 transcripts, and absence of α₂δ-1 protein detected in patient-derived fibroblasts. Patient 2 is compound heterozygous for an early frameshift variant c.13_23dup/p.(Leu9Alafs*5), highly probably representing a null allele and a missense variant c.626G>A/p.(Gly209Asp). Our functional studies show that this amino-acid change severely impairs the function of α₂δ-1 as a calcium channel subunit, with strongly reduced trafficking of α₂δ-1^{G209D} to the cell surface and a complete inability of α₂δ-1^{G209D} to increase the trafficking and function of Ca_v2 channels. Thus, biallelic loss-of-function variants in CACNA2D1 underlie the severe neurodevelopmental disorder in these two patients. Our results demonstrate the critical importance and non-interchangeability of α₂δ-1 and other α₂δ proteins for normal human neuronal development.

- 1 Department of Neuroscience Physiology and Pharmacology, University College London (UCL), London WC1E 6BT, UK
- 2 Institute of Human Genetics, University Medical Center Hamburg-Eppendorf, 20246 Hamburg, Germany
- 3 Neurology and Neurological Sciences, Pediatrics, Division of Medical Genetics, Stanford University and Lucile Packard Children's Hospital, Palo Alto, CA 94304, USA
- 4 Department of Microbiology and Translational Data Analytics Institute, The Ohio State University, Columbus, OH, 43210, USA
- 5 Department of Molecular and Human Genetics, Baylor College of Medicine/NGS-Molecular, Baylor Genetics, Houston, TX, USA

Correspondence to: Annette C. Dolphin
Department of Neuroscience Physiology and Pharmacology
University College London (UCL)
Gower St., London WC1E 6BT, UK
E-mail: a.dolphin@ucl.ac.uk

Received November 23, 2021. Revised January 26, 2022. Accepted February 13, 2022. Advance access publication March 16, 2022

© The Author(s) 2022. Published by Oxford University Press on behalf of the Guarantors of Brain.

This is an Open Access article distributed under the terms of the Creative Commons Attribution License (<https://creativecommons.org/licenses/by/4.0/>), which permits unrestricted reuse, distribution, and reproduction in any medium, provided the original work is properly cited.

Correspondence may also be addressed to: Kerstin Kutsche
Institute of Human Genetics University Medical Center
Hamburg-Eppendorf, 20246 Hamburg, Germany
E-mail: kkutsche@uke.de

Keywords: epileptic encephalopathy; calcium channel; loss-of-function; biallelic variants; *CACNA2D1*

Abbreviations: DEE = developmental and epileptic encephalopathy; GFP = green fluorescent protein

Introduction

Voltage-gated calcium (Ca_v) channels are present in all excitable cells including neurons, and open following membrane depolarization, allowing Ca^{2+} entry.¹ The α_1 pore-forming subunits are encoded by a family of 10 mammalian genes, divided into three subfamilies (Ca_v1 – 3).¹ In neurons, Ca_v2 channels are mainly presynaptic and involved in synaptic transmission.²

The Ca_v1 and Ca_v2 subfamilies are associated with auxiliary $\text{Ca}_v\beta$ and $\alpha_2\delta$ subunits.² The $\alpha_2\delta$ proteins are encoded by four mammalian genes, *CACNA2D1*–*4*,² encoding an $\alpha_2\delta$ pre-protein that is post-translationally cleaved into two polypeptides, α_2 and δ .³ These extracellular glycoproteins remain disulphide-bonded together, linked into the plasma membrane by a glycosylphosphatidylinositol anchor.⁴ Human $\alpha_2\delta$ -1 pre-protein (P54289, UniProt) has 1103 amino acids. In conjunction with β , the $\alpha_2\delta$ subunits play important roles in trafficking and function of Ca_v1 and Ca_v2 channels.⁵

Evidence that $\alpha_2\delta$ proteins are involved in neurological disease has been reviewed recently.⁶ Initial evidence was for $\alpha_2\delta$ -2, and came from the spontaneous *Cacna2d2* mouse mutant strains including *ducky*,⁷ which demonstrate absence epilepsy and severe cerebellar ataxia when both alleles are mutated. This reflects the strong expression of $\alpha_2\delta$ -2 in particular neurons, specifically cerebellar Purkinje cells.⁷ In humans, biallelic *CACNA2D2* variants cause a phenotypic spectrum ranging from congenital ataxia with cerebellar vermal atrophy on brain imaging⁸ to cerebellar atrophy and developmental and epileptic encephalopathies (DEEs).^{9,10} DEEs are characterized by intractable seizures and developmental impairment or regression.¹¹

Here we report two unrelated patients with biallelic *CACNA2D1* variants, one with a homozygous frameshift variant and the other with compound heterozygosity for an early frameshift and a missense variant. Both individuals show a highly consistent phenotype, corresponding to DEE. We demonstrate that the homozygous frameshift variant causes $\alpha_2\delta$ -1 loss in patient fibroblasts, and investigate the effect of the $\alpha_2\delta$ -1 amino-acid change p.(Gly209Asp) on calcium channel function. Our data indicate that biallelic loss-of-function variants in *CACNA2D1* underlie this DEE.

Materials and methods

Patients

Informed consent for genetic analyses was obtained for the two patients. Genetic studies were performed clinically or as approved by the Institutional Review Boards of the relevant institutions (Ethics Committee, Hamburg Medical Chamber; PV3802). The patients' parents provided written informed consent for study participation, clinical data and specimen collection, genetic analysis and publication of relevant findings.

Exome sequencing, analysis and variant validation

Genomic DNA was extracted from peripheral blood samples using standard procedures. We performed trio exome sequencing with DNA samples of Patient 1 and both healthy parents ([Supplementary material](#)). Primer sequences are in [Supplementary Table 1](#). For Patient 2, trio exome sequencing was undertaken with DNA samples of the proband and both healthy parents at Baylor Genetics ([Supplementary material](#)).

RNA isolation and transcript analysis

RNA isolation from fibroblasts, complementary DNA synthesis, polymerase chain reaction (PCR) and Sanger sequencing of amplicons to analyse *CACNA2D1* transcripts were performed as described.¹² Quantitative PCR to determine the relative mRNA levels of *CACNA2D1* and *CACNA2D3* was performed as described.¹² Primer sequences are in [Supplementary Table 1](#).

Bioinformatic analysis of *CACNA2D1* homologues

Details of bioinformatic analysis are described in the [Supplementary material](#).

Cell culture and antibodies

Primary fibroblasts, tsA-201 cells and hippocampal neurons were cultured as described ([Supplementary material](#)). The antibodies used are described in [Supplementary material](#).

Immunoblot analysis of fibroblasts

Whole-cell lysates from patient and control fibroblasts were prepared, and immunoblotting performed as described¹² ([Supplementary material](#)).

Expression constructs, mutagenesis and cell transfection

Details of expression constructs, transfection markers and procedures are detailed in [Supplementary material](#). The tsA-201 cells were transfected with PolyJet or Fugene6 (as stated) according to manufacturers' protocols. Hippocampal neurons were transfected with Lipofectamine 2000 (Life Technologies).

Electrophysiology

$\text{Ca}_v2.1$ and $\text{Ca}_v2.2$ currents in transfected tsA-201 cells were investigated by whole-cell patch-clamp recording ([Supplementary material](#)).

Table 1 Family history, growth parameters and manifestation of first symptoms in patients with biallelic CACNA2D1 variants

	Patient 1	Patient 2
Ethnicity	Afghan	Caucasian, Native American
Parental consanguinity	First cousins	No
Family history	Epileptic encephalopathy in paternal uncle	No
Sex	Male	Male
CACNA2D1 variants (NM_000722.3)	c.818_821dup/p.(Ser275Asnfs*13) homozygous	c.13_23dup/p.(Leu9Alafs*5) and c.626G>A/p.(Gly209Asp) compound heterozygous
Pregnancy	Uncomplicated	Uncomplicated
Birth at	37 weeks, uncomplicated	40 weeks
Birth weight, g/z-score	2960/−0.5	3345/−0.73
Birth length, cm/z-score	50/−0.2	Unknown
OFC at birth, cm/z-score	33/−1.0	Unknown
Age at last examination	4 years 11 months	4 years
Weight at last examination, kg/z-score	18/−0.4	15.5/−0.52
Length at last examination, cm/z-score	110/−0.2	97.8/−0.68
OFC at last examination, cm/z-score	48.9/−2.1	47.5/−2.02
Manifestation		
First symptoms at age of	3 months	<2 months
First clinical signs	Severe hypotonia with poor head control, no visual attention	Hypotonia with poor head control, decreased visual attention

Cell surface biotinylation, co-immunoprecipitation and immunocytochemistry

Cell surface biotinylation, co-immunoprecipitation, immunoblotting and immunocytochemistry was performed as described in Kadurin et al.¹³ (Supplementary material).

Data analysis and availability

Data analysis and availability are described in Supplementary material.

Results

Biallelic variants in CACNA2D1 in two unrelated individuals with DEE

Through GeneMatcher,¹⁴ we identified the two unrelated male individuals, Patients 1 and 2, with a highly consistent phenotype corresponding to DEE. The two affected individuals carried biallelic pathogenic variants in CACNA2D1 (Tables 1 and 2). Patient 1 developed generalized seizures at age 19 months, while onset of epilepsy was at age 11.5 months in Patient 2. At last examination, Patient 1 was 4 years 11 months and Patient 2 was 4 years old. Both were microcephalic, had severe hypotonia, absent speech, spasticity, choreiform movements, orofacial dyskinesia and cortical visual impairment (Tables 1 and 2, and case reports in the Supplementary material). Brain imaging revealed corpus callosum hypoplasia and progressive volume loss in both (Fig. 1A and B). Patient 1 had no cardiac anomalies, while a tiny patent foramen ovale was found in Patient 2 (Tables 1 and 2).

Trio exome sequencing in Patient 1 and parents revealed in the proband the homozygous CACNA2D1 (NM_000722.3) frameshift variant c.818_821dupGAAC/p.(Ser275Asnfs*13). The variant is absent from public databases including gnomAD (v.2.1.1 and 3.1.1). The 4-bp duplication was validated in Patient 1's DNA and fibroblast-derived complementary DNA. His healthy parents were heterozygous carriers (Tables 1 and 2 and Supplementary Fig. 1). In Patient 2, trio

exome sequencing demonstrated compound heterozygosity for the CACNA2D1 variants c.13_23dupTGCCTGCTGGC [p.(Leu9Alafs*5)] and c.626G>A [p.(Gly209Asp)] (Tables 1 and 2 and Supplementary Fig. 1). His healthy mother was heterozygous for the c.13_23dup TGCCTGCTGGC variant and his healthy father for the c.626G>A variant. The 11-bp duplication is probably a loss-of-function variant; it has a worldwide minor allele frequency of 0.003% (gnomAD v.2.1.1), while the c.626G>A variant is absent in gnomAD (v.2.1.1 and 3.1.1). The missense variant c.626G>A/p.(Gly209Asp) in exon 7 is predicted to be damaging by *in silico* tools detailed in Supplementary material.

In fibroblasts of Patient 1, CACNA2D1 mRNA level was reduced to 6–9% compared with control fibroblasts, while it was similar in Patient 2 and control fibroblasts (Fig. 1C and Supplementary Fig. 2). We next determined $\alpha_2\delta$ -1 levels in whole-cell lysates from cultured primary fibroblasts of Patients 1 and 2. Qualitatively, we detected little full-length $\alpha_2\delta$ -1 in Patient 1 fibroblasts, while it was present in Patient 2 and control cells (Fig. 1D and Supplementary Fig. 3). Quantification of $\alpha_2\delta$ -1 indicated 10–12% in Patient 1 and 31–38% in Patient 2 compared to controls (Fig. 1E). Together, these data indicate that Patient 1 carries biallelic CACNA2D1 loss-of-function alleles and Patient 2 harbours at least one CACNA2D1 loss-of-function variant.

Next, we investigated mRNA levels of the other CACNA2D genes in patient fibroblasts to identify possible compensatory effects. While mRNA levels of CACNA2D2 and CACNA2D4 were too low to be quantified, we detected 3- to 7-fold higher CACNA2D3 mRNA levels in Patient 2 fibroblasts compared to Patient 1 and control cells (Supplementary Fig. 4).

Glycine 209 is invariant in CACNA2D1

The $\alpha_2\delta$ -1 protein (also denoted as CACNA2D1) contains a von Willebrand factor-A domain and four Ca²⁺ channel and chemotaxis receptor (Cache) domains,¹⁵ organized into two double-Cache (dCache) domains.¹⁶ The p.(Gly209Asp) (G209D) amino-acid substitution in the CACNA2D1 gene product of Patient 2 is within the gabapentin and amino-acid binding pocket of its dCache₁

Table 2 Neurological and other findings in patients with biallelic CACNA2D1 variants

Neurological signs		
Global developmental delay	Profound	Profound
Motor skills	No achievement of motor milestones	Rolls to one side, reaches for toys intermittently
Muscular hypotonia	Severe axial, insufficient head control	Markedly low axial tone, appendicular tone is also low, increased with activation
Spasticity	In all extremities, starting at 2 years	Hands often fisted since birth, spastic catch at elbows and knees more prominent over time, back arching episodes beginning <12 months
Dystonic movements	Choreiform movements of upper extremities, orofacial dyskinesia, onset <2 years	Distal choreiform movements of all extremities, orofacial dyskinesia and generalized dystonic episodes, onset <10 months
Intellectual disability	Profound	Profound
Speech impairment	Profound	Profound
Behaviour	No concerns	No concerns
Cerebral MRI	Hypoplastic corpus callosum, enlarged inner and outer CSF spaces at age 7 months; progressive frontotemporal and mesial temporal atrophy at 4 years 10 months	Generalized volume loss, borderline thinning of the corpus callosum at 11 months; progression of generalized volume loss at 26 months
Hearing	Normal, not tested	Normal
Eyes	Cortical visual impairment, nystagmus	Cortical visual impairment, intermittent disconjugate gaze
Seizures		
Age of onset	9 months: absences; 19 months: generalized seizures	11 months: right face/arm twitching, abnormal EEG
Initial seizure type	Absences, generalized	Focal with impaired awareness (hemi-clonic), atypical absence
Current seizure type	Absences	Focal with impaired awareness (hemi-clonic), 3 years 9 months: ESES
Response to treatment	Well (generalized seizures), poor (absences)	Well controlled on Depakene
EEG	Normal at age 7 months	11 months: diffusely slow, no anterior posterior frequency amplitude gradient, slow spike and wave in sleep, multifocal spikes. Focal motor seizure captured, some irregular generalized spikes with possible eye blinking and unresponsive. 3 years 9 months: mild diffuse slowing, occasional multifocal sharps and 2–3 Hz spike and wave during wakefulness, near continuous slow spike and wave during sleep meeting criteria for ESES
Feeding		
Feeding difficulties	G tube placement at 4 years	Since birth, s/p G tube placement at 13 months
Cardiac features		
Echocardiography	Normal	Limited study with tiny patent foramen ovale, normal function
Electrocardiography	Normal	Normal, including 24 h patch recording
Other findings		
Facial dysmorphism	Bitemporal narrowing, large ears, flared medial eyebrows, open mouth with tented upper lip	Microcephalic with posterior plagiocephaly, mild bitemporal narrowing, ears are low set and appear larger relative to head size, mild ptosis bilaterally, mouth held hanging open, high arched palate, teeth are widely spaced and blunted due to frequent bruxism, small hands and feet
Sleep disturbance	Yes	Obstructive sleep apnoea
Insensibility to pain	Yes	Yes

ESES = electrical status epilepticus in sleep; s/p = status post.

domain.¹⁶ This Gly residue is important for maintaining a three-strand beta-sheet stability and simultaneously providing a critical turn in the structure. G209 is absolutely invariant in both CACNA2D1 and CACNA2D2 orthologues in all vertebrates and paralogues and predecessors from low invertebrates (Supplementary Fig. 5).

The p.(Gly209Asp) variant disrupts plasma membrane $\alpha_2\delta$ -1 expression

We then investigated the *in vitro* effect of the p.(Gly209Asp) variant on $\alpha_2\delta$ -1 as a calcium channel subunit. First, we compared cell surface expression of wild-type HA- $\alpha_2\delta$ -1 (HA- $\alpha_2\delta$ -1 WT) and

HA- $\alpha_2\delta$ -1^{G209D} in non-permeabilized cells.⁵ As shown by the haemagglutinin (HA) signal, the expression of HA- $\alpha_2\delta$ -1^{G209D} at the cell surface was reduced by ~80% compared to HA- $\alpha_2\delta$ -1 WT (Fig. 2A and B). In agreement, cell surface biotinylated HA- $\alpha_2\delta$ -1^{G209D} was decreased, by 86.2%, compared to HA- $\alpha_2\delta$ -1 WT (Fig. 2C and D).

The p.(Gly209Asp) variant abolishes ability of $\alpha_2\delta$ -1 to promote $\text{Ca}_v2.2$ currents

$\text{Ca}_v2.2$ currents were then measured in tsA-201 cells transfected with HA-tagged $\text{Ca}_v2.2$ with $\beta 1b$ and $\alpha_2\delta$ -1 wild-type, $\alpha_2\delta$ -1^{G209D} or no $\alpha_2\delta$. While $\alpha_2\delta$ -1 wild-type increased $\text{Ca}_v2.2$ currents by ~13-fold, $\alpha_2\delta$ -1^{G209D} produced no increase compared to without

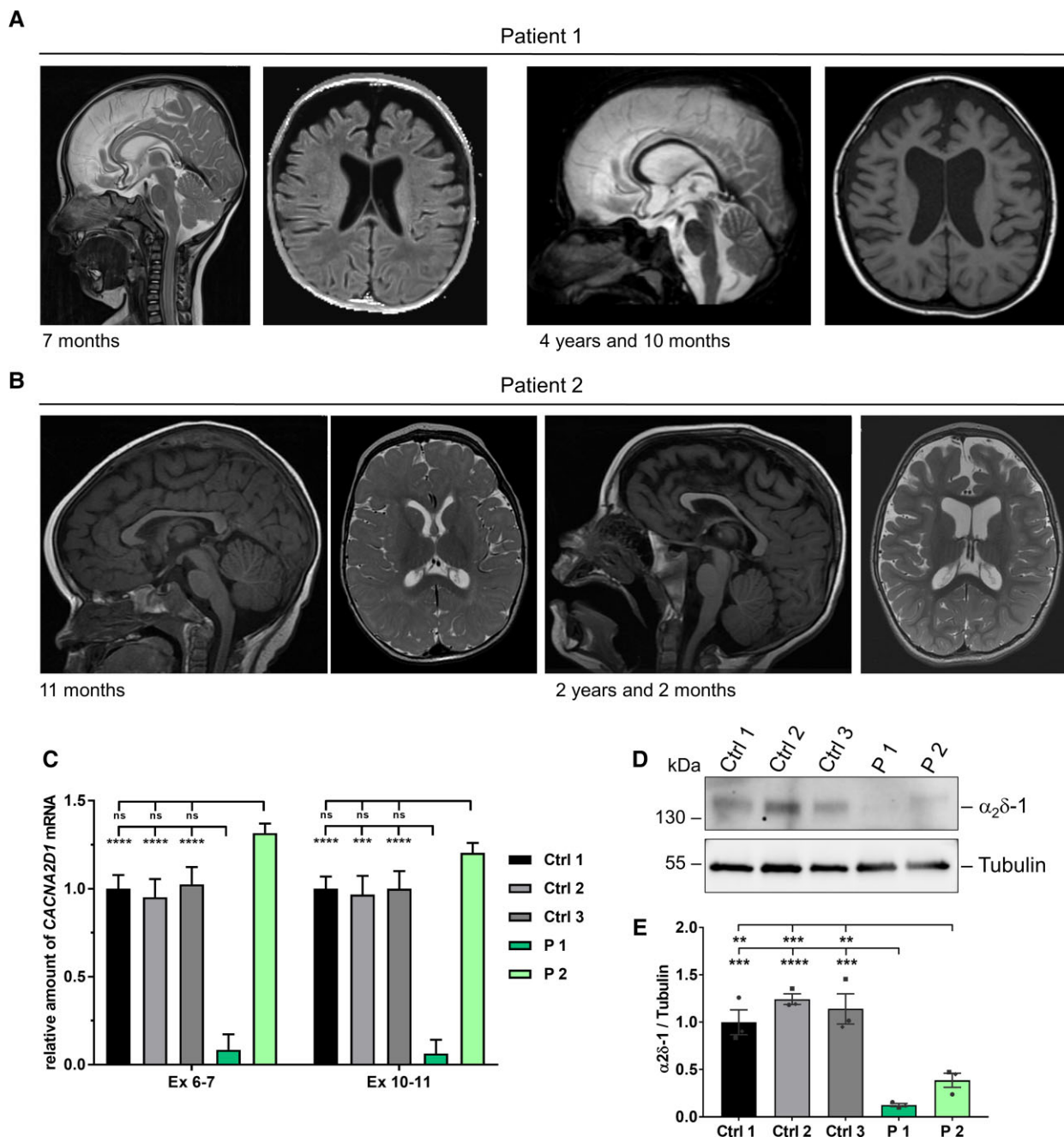


Figure 1 MRI scans of patients with biallelic variants in *CACNA2D1* and determination of *CACNA2D1* mRNA and $\alpha_2\delta-1$ protein levels in patient-derived fibroblasts. (A) In Patient 1, T₂-weighted sagittal MRI shows hypoplastic corpus callosum and T₁-weighted axial image shows enlarged ventricles and frontotemporal CSF spaces at the age of 7 months. At the age of 4 years and 10 months, progressive frontotemporal and mesial temporal atrophy was noted. (B) At the age of 11 months, T₁-weighted sagittal and T₂-weighted axial MRI images of Patient 2 show non-specific findings of delayed myelination within the frontal and parietal white matter for age and prominent perivascular spaces. At the age of 26 months, T₁-weighted sagittal MRI shows interval generalized volume loss with extra-axial spaces and thinning of the corpus callosum. T₂-weighted axial images show an increase in ventricular size in addition to increased intra-axial spaces. Permission to publish MRI scans was provided for the two patients shown here. (C) Relative quantification of *CACNA2D1* transcripts by reverse transcription-qPCR (RT-qPCR) using two *CACNA2D1*-specific primer pairs generating amplicons for exons 6–7 and 10–11. RNA was obtained from fibroblasts of Patients 1 and 2 and three healthy individuals (Controls 1–3). Glyceraldehyde-3-phosphate dehydrogenase (GAPDH) mRNA was used as an internal control; and the amount of target mRNA relative to GAPDH mRNA is presented. Mean \pm standard error of the mean (SEM) of three independent experiments, each performed in triplicate, is shown. One-way ANOVA with Bonferroni *post hoc* test for multiple comparisons was used for statistical analysis: ns, $P > 0.05$; *** $P = 0.0001$; **** $P < 0.0001$. Datasets of independent RT-qPCR experiments with technical triplicates are shown in [Supplementary Fig. 2](#). (D) Representative immunoblot of whole-cell lysates obtained from fibroblasts of Patients 1 and 2 and three controls. The amount of $\alpha_2\delta-1$ was monitored with an anti- $\alpha_2\delta-1$ antibody. An anti-tubulin antibody was used to demonstrate equal loading. A band corresponding to $\alpha_2\delta-1$, which shows a low expression in fibroblasts, was observed in all control cells. Uncropped blots are shown in [Supplementary Fig. 3](#). (E) Band intensities were quantified using the ChemiDoc imaging system. Mean \pm SEM with individual data-points of three independent experiments is shown. One-way ANOVA followed by a Bonferroni *post hoc* test for multiple comparisons was used for statistical analysis: ** $P < 0.0065$; *** $P < 0.0005$; **** $P < 0.0001$. Ctrl = control; ex = exon; ns = not significant; P = patient.

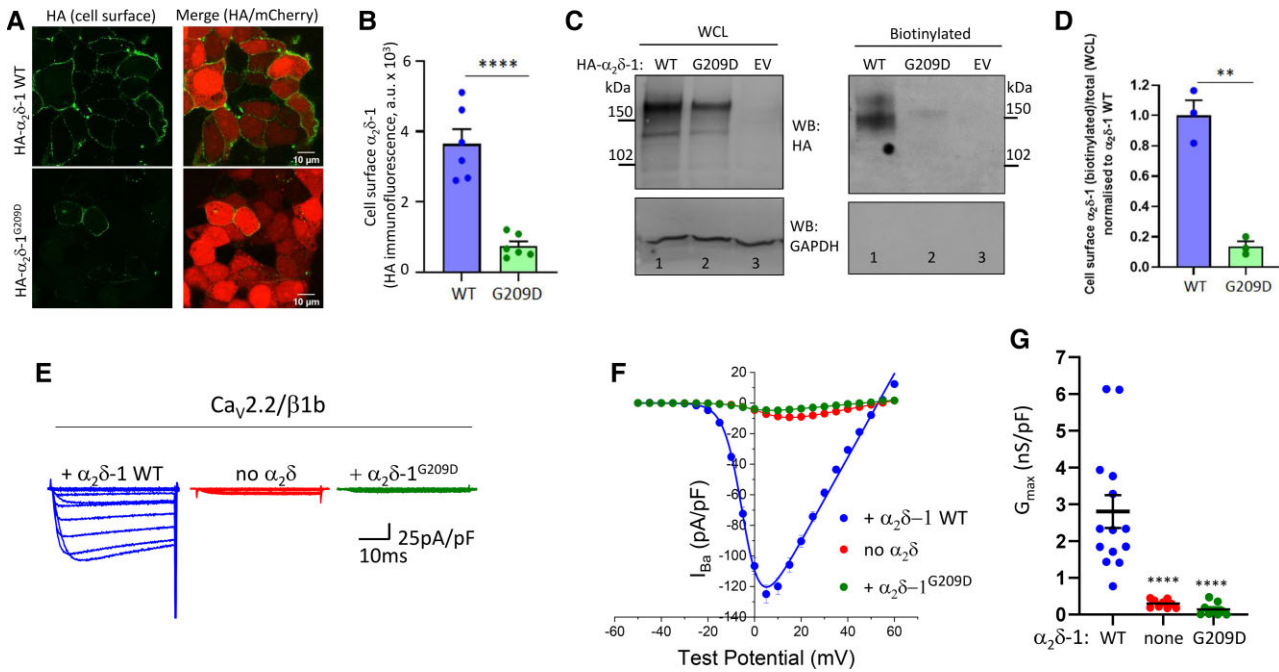


Figure 2 The p.(Gly209Asp) variant disrupts $\alpha_2\delta$ -1 expression at the cell surface, and does not promote Ca_v2 calcium currents. (A) Representative confocal images of tsA-201 cells transfected with either HA- $\alpha_2\delta$ -1 wild-type (WT) or HA- $\alpha_2\delta$ -1^{G209D} with mCherry. HA staining was performed in non-permeabilized conditions and shown in the left panels. The right panels represent the merged images with the 10 μm scale bar. (B) Bar charts (mean \pm SEM with individual data-points, each representing mean of at least 60 cells) showing the expression at the cell surface (HA signal) of WT $\alpha_2\delta$ -1-HA (blue bar) and HA- $\alpha_2\delta$ -1^{G209D} (green bar). Data obtained from six coverslips in two independent experiments, **** $P < 0.0001$, Student's t-test. (C) Western blot experiments for HA- $\alpha_2\delta$ -1 (anti-HA Ab, top; molecular weight ~ 140 – 170 kDa for the glycosylated uncleaved and proteolytically cleaved $\alpha_2\delta$ -1 proteins) and GAPDH (used as a control, bottom). Left panels show whole-cell lysate (WCL) input and right panels show cell surface biotinylated samples from tsA-201 cells transfected with HA- $\alpha_2\delta$ -1 WT (lane 1) or HA- $\alpha_2\delta$ -1^{G209D} (lane 2) or empty vector (EV, lane 3). Western blots were performed under reducing conditions, such that the disulphide bonds between α_2 and δ were broken. Uncropped blots are in [Supplementary Fig. 10A](#). (D) Mean \pm SEM and individual data-points of cell surface HA- $\alpha_2\delta$ -1 WT (blue bar) or HA- $\alpha_2\delta$ -1^{G209D} (green bar) measured as a proportion of biotinylated over total protein normalized to HA- $\alpha_2\delta$ -1 WT. ** $P = 0.0012$, Student's t-test. (E) Example of whole-cell patch-clamp recordings for Ca_v2 -HA co-expressed with $\beta 1b$ and either $\alpha_2\delta$ -1 WT (blue, left), empty vector (no $\alpha_2\delta$, red, centre) or $\alpha_2\delta$ -1^{G209D} (green, right). Holding potential -80 mV, steps between -50 and $+60$ mV for 50 ms (applies to all traces). (F) Mean (\pm SEM) IV relationships for the conditions shown in E. Ca_v2 -HA co-expressed with $\alpha_2\delta$ -1 WT ($n = 14$, blue filled circles), empty vector (no $\alpha_2\delta$, $n = 10$, red filled circles) or $\alpha_2\delta$ -1^{G209D} ($n = 10$, green filled circles). The individual and mean data were fit with a modified Boltzmann equation (see 'Materials and methods' section). (G) G_{max} [nanosiemens (nS)/picofarad (pF)] from the IV relationships shown in F. Individual data (same symbols as in F) and mean \pm SEM are plotted. **** $P < 0.0001$ versus wild-type (one-way ANOVA and Sidak's post hoc test correcting for multiple comparisons).

$\alpha_2\delta$ (Fig. 2E–G). Expression of all subunits was confirmed by western blotting and immunocytochemistry ([Supplementary Fig. 6](#)). This effect was not specific to Ca_v2 , as $\alpha_2\delta$ -1^{G209D} also did not increase Ca_v2 currents ([Supplementary Fig. 7A–C](#)).

We next investigated expression of the calcium channel complex at the plasma membrane, using double-tagged GFP- Ca_v2 -HA. When GFP- Ca_v2 -HA was co-expressed with $\alpha_2\delta$ -1 wild-type, this resulted in an increase in its cell surface expression compared with no $\alpha_2\delta$ control (Fig. 3A and B). However, this effect was completely absent when Ca_v2 was co-expressed with $\alpha_2\delta$ -1^{G209D} (Fig. 3A and B).

$\alpha_2\delta$ -1^{G209D} does not promote Ca_v2 cell surface expression or trafficking in hippocampal neurons

Ca_v2 is a neuronal calcium channel, and we therefore investigated the effect of $\alpha_2\delta$ -1^{G209D} on Ca_v2 trafficking in neurons, as previously described.¹³ We first analysed cell surface expression of GFP- Ca_v2 -HA in cultured hippocampal cell bodies. As expected, in the presence of $\alpha_2\delta$ -1 WT, GFP- Ca_v2 -HA was strongly expressed at the cell surface (HA signal, Fig. 3C and D). In contrast, in the presence of $\alpha_2\delta$ -1^{G209D}, GFP- Ca_v2 -HA could not be detected at the cell surface, similar to no $\alpha_2\delta$ (Fig. 3C and D).

The neurites of these cells were then imaged. As expected, GFP- Ca_v2 -HA showed strong expression when co-expressed with $\alpha_2\delta$ -1 WT; this was observed for both HA (cell surface) and green fluorescent protein (GFP) (total Ca_v2) (Fig. 3E and F). In contrast, $\alpha_2\delta$ -1^{G209D} did not promote trafficking of Ca_v2 into hippocampal neurites (Fig. 3E and F). This is indicated by the finding that both HA (cell surface Ca_v2) and GFP (total Ca_v2) signals were reduced in parallel.

$\alpha_2\delta$ -1^{G209D} shows reduced complex formation with Ca_v2 and limited proteolytic cleavage

To examine whether the lack of ability of $\alpha_2\delta$ -1^{G209D} to promote calcium channel function was due to reduced interaction with Ca_v2 , we performed co-immunoprecipitation experiments, using GFP- Ca_v2 -HA (Fig. 4A). For $\alpha_2\delta$ -1 WT, robust interaction was shown by the presence of HA- $\alpha_2\delta$ -1 WT, co-immunoprecipitated by GFP- Ca_v2 -HA, using anti-GFP antibody (Fig. 4A, lane 6). In contrast, very weak co-immunoprecipitation was observed for HA- $\alpha_2\delta$ -1^{G209D} (Fig. 4A, lane 7), quantified in Fig. 4B. As a control, there was no co-immunoprecipitation of HA- $\alpha_2\delta$ -1 WT using Ca_v2 -HA without a GFP tag (Fig. 4A, lane 5).

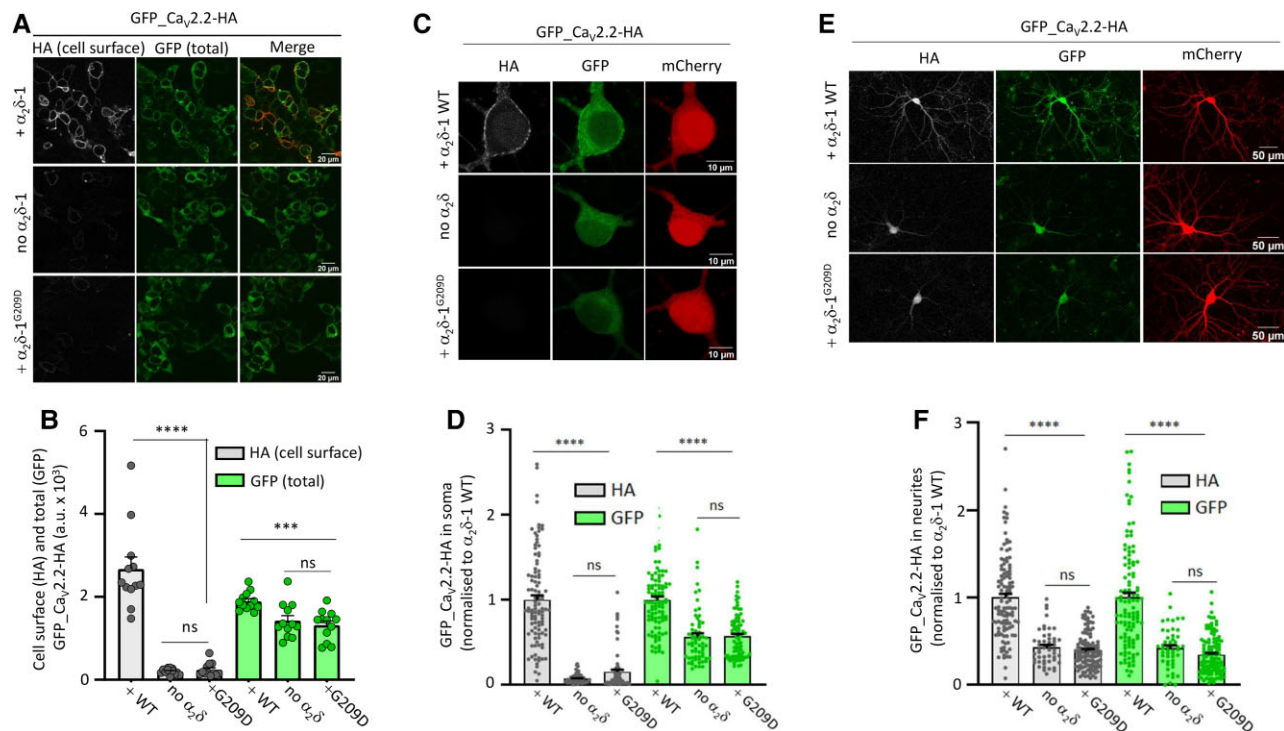


Figure 3 $\alpha_2\delta$ -1^{G209D} does not enhance Ca_v2.2 expression at the cell surface in tsA-201 cells and hippocampal neurons. (A) Representative confocal images of tsA-201 cells transfected with GFP_Ca_v2.2-HA with either $\alpha_2\delta$ -1 wild-type (WT) (without tag; top row), empty vector (no $\alpha_2\delta$, middle row) or $\alpha_2\delta$ -1^{G209D} (without tag; bottom row). HA staining was performed in non-permeabilized conditions (white, left), GFP signal shows total Ca_v2.2 (middle, left). The right panels represent the merged images (HA is shown in red). Scale bar = 20 μ m. (B) Bar charts (mean \pm SEM with individual data-points representing the mean of at least 50 cells from 12 coverslips) show Ca_v2.2 expressed at the cell surface (HA signal, grey bars) or total Ca_v2.2 (GFP, green bars) in the presence of $\alpha_2\delta$ -1 WT, empty vector (no $\alpha_2\delta$ -1) or $\alpha_2\delta$ -1^{G209D}. Data obtained from four independent experiments; ns, $P > 0.05$; **** $P = 0.0007$, **** $P < 0.0001$, one-way ANOVA and Bonferroni post hoc test. (C) Representative confocal images of hippocampal somata imaged at $\times 63$ objective and transfected with GFP_Ca_v2.2-HA and either $\alpha_2\delta$ -1 WT (top row), empty vector (no $\alpha_2\delta$, middle row) or $\alpha_2\delta$ -1^{G209D} (bottom row) together with $\beta 1b$ and mCherry. HA staining was performed in non-permeabilized conditions (grey, left), GFP signal (middle) and mCherry (transfection marker, right). Scale bar = 10 μ m. (D) Bar charts (mean \pm SEM with individual data-points) of HA (grey bars) and GFP (green bars) for $\alpha_2\delta$ -1 WT ($n = 102$), no $\alpha_2\delta$ ($n = 63$) and $\alpha_2\delta$ -1^{G209D} ($n = 82$). Data obtained from three independent experiments; the values are normalized to $\alpha_2\delta$ -1 WT condition in each experiment. ns, $P > 0.05$; **** $P < 0.0001$, one-way ANOVA and Bonferroni post hoc test. (E) Representative confocal images of hippocampal neurons imaged at $\times 20$ objective and transfected with GFP_Ca_v2.2-HA and either $\alpha_2\delta$ -1 WT (top row), empty vector (no $\alpha_2\delta$, middle row) or $\alpha_2\delta$ -1^{G209D} (bottom row) together with $\beta 1b$ and mCherry. HA staining was performed in non-permeabilized conditions (grey, left panels), GFP signal (middle) and mCherry (transfection marker, right). Scale bar = 50 μ m. (F) Bar charts (mean \pm SEM with individual data-points) of HA (grey bars) and GFP (green bars) for $\alpha_2\delta$ -1 WT ($n = 114$), no $\alpha_2\delta$ ($n = 50$) and $\alpha_2\delta$ -1^{G209D} ($n = 117$). Data obtained from three independent experiments; the values are normalized to $\alpha_2\delta$ -1 WT condition in each experiment. ns, $P > 0.05$; **** $P < 0.0001$, one-way ANOVA and Bonferroni post hoc test. Note that for B, D and F, total Ca_v2.2 (GFP) was reduced in both the $\alpha_2\delta$ -1^{G209D} and no $\alpha_2\delta$ conditions compared to $\alpha_2\delta$ -1 WT condition probably because of its increased degradation when Ca_v2.2 is poorly trafficked out of the endoplasmic reticulum.

Interestingly, co-immunoprecipitated HA- $\alpha_2\delta$ -1^{G209D} (Fig. 4A, lane 7, arrow) had a noticeably higher apparent molecular weight compared to HA- $\alpha_2\delta$ -1 WT (lane 6), and we found this was due to almost complete lack of proteolytic cleavage of HA- $\alpha_2\delta$ -1^{G209D} into α_2 and δ (Supplementary material and Supplementary Fig. 8).

In summary, these results show that $\alpha_2\delta$ -1^{G209D} remains largely as the uncleaved immature form, indicating that it probably remains in the endoplasmic reticulum. In agreement with our previous results for uncleaved $\alpha_2\delta$ -1,¹⁷ it shows much less complex formation with Ca_v2.2. This result suggested that $\alpha_2\delta$ -1^{G209D} would be unlikely to interfere with other $\alpha_2\delta$ proteins interacting with Ca_v2.2. In agreement with this, we found that $\alpha_2\delta$ -1^{G209D} did not affect the ability of $\alpha_2\delta$ -3 to enhance Ca_v2.2 currents (Supplementary Fig. 9A–C). This result underscores that the p.(Gly209Asp) variant has a loss-of-function effect.

Discussion

In the current study, we show that biallelic loss-of-function variants in CACNA2D1 underlie DEE. In Patient 1 the homozygous

frameshift variant p.(Ser275Asnfs*13) causes nonsense-mediated mRNA decay of mutated CACNA2D1 transcripts and absence of $\alpha_2\delta$ -1 in patient-derived fibroblasts. The variants p.(Leu9Alafs*5) and p.(Gly209Asp) in Patient 2 are a combination of a very early frameshift and a missense variant in trans, with the latter severely affecting Ca_v2 calcium channel function.

Our electrophysiological, biochemical and immunocytochemistry data show that $\alpha_2\delta$ -1^{G209D} is completely non-functional, in that, unlike wild-type $\alpha_2\delta$ -1,⁵ it traffics extremely poorly to the cell surface, and does not enhance the function or trafficking of Ca_v2 channels in both non-neuronal cells and hippocampal neurons. Furthermore, $\alpha_2\delta$ -1^{G209D} shows markedly reduced cleavage into α_2 and δ , an enzymatic process that normally begins in the Golgi apparatus.^{13,17} This suggests that $\alpha_2\delta$ -1^{G209D} does not traffic beyond the endoplasmic reticulum. Our previous finding that an uncleavable mutant $\alpha_2\delta$ -1 shows lower association with the Ca_v2.2 α_1 subunit than the mature cleaved $\alpha_2\delta$ -1,¹⁷ indicates that the lack of proteolytic cleavage of $\alpha_2\delta$ -1^{G209D} will probably contribute to the observed reduction in interaction of $\alpha_2\delta$ -1^{G209D} with the Ca_v2.2 α_1 subunit. This demonstrates the importance of a detailed understanding of $\alpha_2\delta$ -1

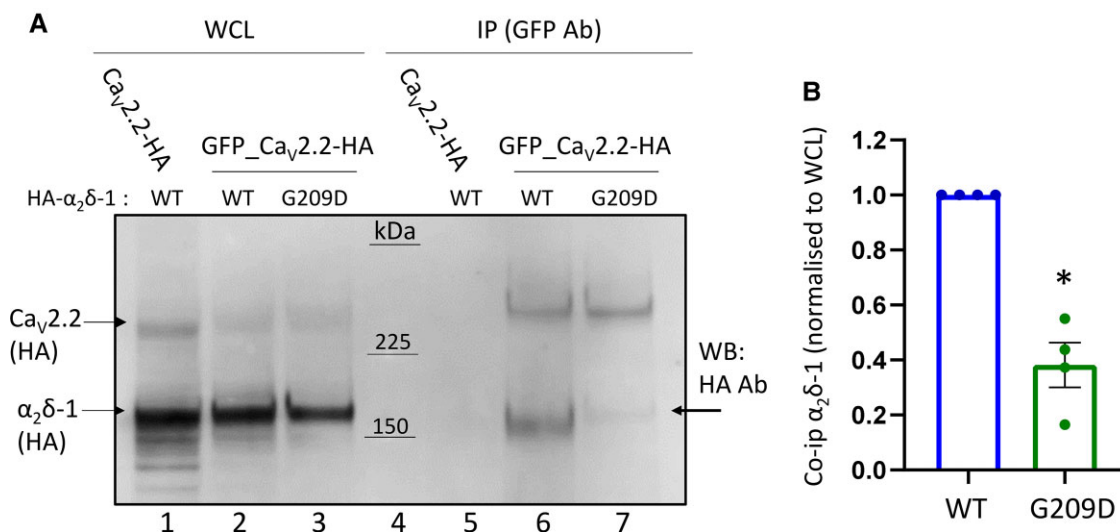


Figure 4 $\alpha_2\delta-1^{G209D}$ shows reduced interaction with $\text{Ca}_V2.2$. (A) GFP- $\text{Ca}_V2.2$ -HA was co-expressed with $\beta 1b$ and either HA- $\alpha_2\delta-1$ WT or HA- $\alpha_2\delta-1^{G209D}$. Both $\text{Ca}_V2.2$ and $\alpha_2\delta-1$ proteins were detected in the same western blot using anti-HA antibodies. Immunoblots of whole-cell lysates (WCL) input (left) and immunoprecipitated (IP using GFP antibodies) samples (right) from tsA-201 cells transfected with $\text{Ca}_V2.2$ -HA, $\beta 1b$ and HA- $\alpha_2\delta-1$ WT (lanes 1 and 5) or GFP- $\text{Ca}_V2.2$ -HA with either HA- $\alpha_2\delta-1$ WT (lanes 2 and 6) or HA- $\alpha_2\delta-1^{G209D}$ (lanes 3 and 7). Immunoblots with anti-HA antibody reveal $\text{Ca}_V2.2$ -HA and GFP- $\text{Ca}_V2.2$ -HA (top bands) and HA- $\alpha_2\delta-1$ WT and HA- $\alpha_2\delta-1^{G209D}$ (lower bands). Immunoprecipitation was performed with anti-GFP antibody to pull down GFP- $\text{Ca}_V2.2$ -HA and the co-immunoprecipitated $\alpha_2\delta-1$ is shown below this on the same blot. $\text{Ca}_V2.2$ -HA lacking GFP tag, used as a negative control, shows a lack of co-immunoprecipitation (co-IP) with HA- $\alpha_2\delta-1$ WT (lane 5). Arrow (lane 7) indicates increased molecular weight of $\alpha_2\delta-1^{G209D}$ relative to $\alpha_2\delta-1$ WT. Western blots were performed under reducing conditions, such that the disulphide bonds between α_2 and δ were broken. Uncropped blots are in [Supplementary Fig. 10B](#). (B) Mean \pm SEM and individual data-points for co-immunoprecipitation of HA $\alpha_2\delta-1$ WT (blue bar) or $\alpha_2\delta-1^{G209D}$ (green bar) measured as a proportion of total protein (whole-cell lysates) and normalized to HA- $\alpha_2\delta-1$ WT. * $P=0.0281$ (ratio paired t-test on non-normalized data).

processing and function, in order to identify the basis for such deleterious variants.

Variants in *CACNA2D1* have previously been associated with cardiac phenotypes in both humans and mice. Homozygous knock-out of *Cacna2d1* in mice resulted in a mild cardiac phenotype and reduced ventricular myocyte calcium current density.¹⁸ These mice also showed peripheral sensory deficits and delayed development of neuropathic pain-related responses.¹⁹ Relevant to this, both patients showed insensitivity to pain ([Table 2](#)). Transgenic mice constitutively over-expressing $\alpha_2\delta-1$ have no gross nervous system defects.²⁰ However, they show spontaneous epileptiform EEG abnormalities and behavioural arrest,²¹ suggesting that not only the spatial and temporal expression but also the expression strength of $\alpha_2\delta-1$ is critical for proper functioning of the mouse brain. Indeed, $\alpha_2\delta-1$ is the major $\alpha_2\delta$ isoform in rodent cerebral cortex.²² Furthermore, an auto-antibody recognizing $\alpha_2\delta-1$ is found in cases of autoimmune encephalitis²³ and amyotrophic lateral sclerosis associated with type 2 diabetes.²⁴

In humans, heterozygous variants in *CACNA2D1* have previously been associated with inherited arrhythmogenic disease, including Brugada²⁵ and short QT²⁶ syndromes, as well as infantile spasms²⁷ and intellectual disability and epilepsy.²⁸ Re-evaluation of these monoallelic variants, together with genetic data presented here give rise to reasonable doubt about an association of these *CACNA2D1* variants with disease ([Supplementary material](#)).

Pathogenic variants in genes encoding several Ca_V channels have been associated with neurological diseases in humans, ranging from early-onset severe spinocerebellar ataxia with neurodevelopmental deficits to DEE (see [Supplementary material](#)). In *CACNA2D2*, rare biallelic loss-of-function variation has been

reported in individuals with DEE, corpus callosum hypoplasia, cerebellar atrophy and ataxia.^{9,10} The two unrelated patients reported here show considerable clinical overlap with individuals carrying homozygous *CACNA2D2* loss-of-function variants, such as global developmental delay and/or intellectual disability, epilepsy and hypoplasia of the corpus callosum. However, atrophy of the brain affects the cerebrum in the two affected individuals with *CACNA2D1* variants, whereas cerebellar atrophy was consistently reported in subjects with *CACNA2D2* variants.²⁹ These data indicate that loss of $\alpha_2\delta-1$ or $\alpha_2\delta-2$ cannot be compensated by any of the other $\alpha_2\delta$ subunits during development. In agreement with this, important, non-overlapping roles for specific $\alpha_2\delta$ proteins in synapse formation *in vitro* have been identified recently, some of which may be calcium channel-independent.³⁰

In conclusion, our data demonstrate that biallelic loss-of-function variants in *CACNA2D1* underlie early-onset DEE characterized by microcephaly, profound developmental delay, seizures, visual impairment, truncal hypotonia, limb spasticity and movement disorder. These clinical features are similar to those in previously reported individuals with homozygous *CACNA2D2* null alleles. Individuals with biallelic *CACNA2D1* or *CACNA2D2* variants all have corpus callosum hypoplasia, while patients with *CACNA2D1* variants show progressive cerebral atrophy whereas subjects harbouring *CACNA2D2* variants have cerebellar atrophy. The loss-of-function frameshift nature of two of the three identified *CACNA2D1* variants, together with our functional studies demonstrating a loss-of-function effect for the amino-acid substitution p.(Gly209Asp), confirm disease causation of homozygous and compound heterozygous *CACNA2D1* variants, while also calling into question a causative role of monoallelic *CACNA2D1* variants in intellectual disability, epilepsy and/or inherited arrhythmogenic diseases.

Acknowledgements

We thank the patient families for participation in this study. We further thank Dennis Zornidt and Kanchan Chaggar for skillful technical assistance.

Funding

This study was supported by grants from Wellcome Trust (grant no. 206279/Z\17\Z to A.C.D.), National Institutes of Health (1R35GM131760 to I.B.Z.) and Deutsche Forschungsgemeinschaft (KU 1240/6-2 and KU 1240/10-1 to K.K.)

Competing interests

The authors report no competing interests.

Supplementary material

[Supplementary material](#) is available at *Brain* online.

References

- Catterall WA, Lenaeus MJ, Gamal El-Din TM. Structure and pharmacology of voltage-gated sodium and calcium channels. *Annu Rev Pharmacol Toxicol.* 2020;60:133–154.
- Dolphin AC, Lee A. Presynaptic calcium channels: Specialized control of synaptic neurotransmitter release. *Nat Rev Neurosci.* 2020;21:213–229.
- De Jongh KS, Warner C, Catterall WA. Subunits of purified calcium channels. α_2 and δ are encoded by the same gene. *J Biol Chem.* 1990;265:14738–14741.
- Davies A, Kadurin I, Alvarez-Laviada A, et al. The $\alpha_2\delta$ subunits of voltage-gated calcium channels form GPI-anchored proteins, a posttranslational modification essential for function. *Proc Natl Acad Sci U S A.* 2010;107:1654–1659.
- Cassidy JS, Ferron L, Kadurin I, Pratt WS, Dolphin AC. Functional exofacially tagged N-type calcium channels elucidate the interaction with auxiliary $\alpha_2\delta$ -1 subunits. *Proc Natl Acad Sci USA.* 2014; 111:8979–8984.
- Ablinger C, Geisler SM, Stanika RI, Klein CT, Obermair GJ. Neuronal $\alpha_2\delta$ proteins and brain disorders. *Pflugers Arch.* 2020; 472:845–863.
- Barclay J, Balaguero N, Mione M, et al. Ducky mouse phenotype of epilepsy and ataxia is associated with mutations in the *Cacna2d2* gene and decreased calcium channel current in cerebellar Purkinje cells. *J Neurosci.* 2001;21:6095–6104.
- Valence S, Cochet E, Rougeot C, et al. Exome sequencing in congenital ataxia identifies two new candidate genes and highlights a pathophysiological link between some congenital ataxias and early infantile epileptic encephalopathies. *Genet Med.* 2019;21:553–563.
- Pippucci T, Parmeggiani A, Palombo F, et al. A novel null homozygous mutation confirms *CACNA2D2* as a gene mutated in epileptic encephalopathy. *PLoS ONE.* 2013;8:e82154.
- Edvardson S, Oz S, Abulhijaa FA, et al. Early infantile epileptic encephalopathy associated with a high voltage gated calcium channelopathy. *J Med Genet.* 2013;50:118–123.
- Scheffer IE, Berkovic S, Capovilla G, et al. ILAE classification of the epilepsies: position paper of the ILAE commission for classification and terminology. *Epilepsia.* 2017;58:512–521.
- Schneeberger PE, von Elsnar L, Barker EL, et al. Bi-allelic pathogenic variants in *HS2ST1* cause a syndrome characterized by developmental delay and corpus callosum, skeletal, and renal abnormalities. *Am J Hum Genet.* 2020;107:1044–1061.
- Kadurin I, Ferron L, Rothwell SW, et al. Proteolytic maturation of $\alpha_2\delta$ represents a checkpoint for activation and neuronal trafficking of latent calcium channels. *eLife.* 2016;5:e21143.
- Sobreira N, Schiettecatte F, Valle D, Hamosh A. GeneMatcher: A matching tool for connecting investigators with an interest in the same gene. *Hum Mutat.* 2015;36:928–930.
- Wu J, Yan Z, Li Z, et al. Structure of the voltage-gated calcium channel Cav1.1 at 3.6 Å resolution. *Nature.* 2016;537: 191–196.
- Gumerov VM, Andrianova EP, Matilla MA, et al. Amino acid sensor conserved from bacteria to humans. *Proc Natl Acad Sci U S A.* 2022; 119(10):e2110415119.
- Ferron L, Kadurin I, Dolphin AC. Proteolytic maturation of $\alpha_2\delta$ controls the probability of synaptic vesicular release. *eLife.* 2018;7:e37507.
- Fuller-Bicer GA, Varadi G, Koch SE, et al. Targeted disruption of the voltage-dependent calcium channel $\alpha_2\delta$ -1 subunit. *Am J Physiol Heart Circ Physiol.* 2009;297:H117–H124.
- Patel R, Bauer CS, Nieto-Rostro M, et al. $\alpha_2\delta$ -1 gene deletion affects somatosensory neuron function and delays mechanical hypersensitivity in response to peripheral nerve damage. *J Neurosci.* 2013;33:16412–16426.
- Li CY, Zhang XL, Matthews EA, et al. Calcium channel $\alpha_2\delta$ 1 subunit mediates spinal hyperexcitability in pain modulation. *Pain.* 2006;125:20–34.
- Faria LC, Gu F, Parada I, Barres B, Luo ZD, Prince DA. Epileptiform activity and behavioral arrests in mice overexpressing the calcium channel subunit $\alpha_2\delta$ -1. *Neurobiol Dis.* 2017;102: 70–80.
- Schlick B, Flucher BE, Obermair GJ. Voltage-activated calcium channel expression profiles in mouse brain and cultured hippocampal neurons. *Neuroscience.* 2010;167:786–798.
- Lee ST, Lee BJ, Bae JY, et al. CaV $\alpha_2\delta$ autoimmune encephalitis: A novel antibody and its characteristics. *Ann Neurol.* 2021;89:740–752.
- Shi Y, Park KS, Kim SH, et al. IgGs from patients with amyotrophic lateral sclerosis and diabetes target Ca_v $\alpha_2\delta$ 1 subunits impairing islet cell function and survival. *Proc Natl Acad Sci USA.* 2019; 116:26816–26822.
- Burashnikov E, Pfeiffer R, Barajas-Martinez H, et al. Mutations in the cardiac L-type calcium channel associated with inherited J-wave syndromes and sudden cardiac death. *Heart Rhythm.* 2010;7:1872–1882.
- Templin C, Ghadri JR, Rougier JS, et al. Identification of a novel loss-of-function calcium channel gene mutation in short QT syndrome (SQTS6). *Eur Heart J.* 2011;32:1077–1088.
- Hino-Fukuyo N, Kikuchi A, Arai-Ichinoi N, et al. Genomic analysis identifies candidate pathogenic variants in 9 of 18 patients with unexplained West syndrome. *Hum Genet.* 2015;134:649–658.
- Valentino F, Bruno LP, Doddato G, et al. Exome sequencing in 200 intellectual disability/autistic patients: New candidates and atypical presentations. *Brain Sci.* 2021;11:936.
- Punetha J, Karaca E, Gezdirici A, et al. Biallelic *CACNA2D2* variants in epileptic encephalopathy and cerebellar atrophy. *Ann Clin Transl Neurol.* 2019;6:1395–1406.
- Schöpf CL, Ablinger C, Geisler SM, et al. Presynaptic $\alpha_2\delta$ subunits are key organizers of glutamatergic synapses. *Proc Natl Acad Sci USA.* 2021;118:e1920827118.